ARCHIVE OF MECHANICAL ENGINEERING

DOI: 10.24425/ame.2024.153242 2025, Vol. 72, No. 1, pp. 1–30

Jaime GALLARDO-ALVARADO [1], Jesus H. TINAJERO-CAMPOS[1]

An application of screw theory to the jerk analysis of the PUMA robot

Received 5 May 2024, **Revised** 11 December 2024, **Accepted** 17 December 2024, **Published online** 28 December 2024

Keywords: jerk, singularity, Plücker coordinates, screw theory, PUMA robot

In this paper, the theory of screws is applied to the jerk analysis of the PUMA robot, one of the most popular serial manipulators in history. The higher order kinematic analyses of robot manipulators, such as the acceleration and the jerk, become relevant in improving, among other issues, the performance of robotic manipulators ameliorating the generation of impulsive forces, optimizing the path planning trajectory, reducing the noise, or making it possible to generate smooth trajectories. Numerical applications are provided with the aim to exemplify the versatility of the method of kinematic analysis employed in the contribution. As a consideration for non-experts in the subject, the contribution includes a brief review of the screw theory and its relationship with Plücker coordinates.

1. Introduction

Let us consider an object, for example a particle, constrained to move according to the position vector $\boldsymbol{r}(t)$ that is function of the time t. The instantaneous velocity vector $\boldsymbol{v}(t)$ of the object is defined as the first time derivative of $\boldsymbol{r}(t)$, i.e., $\boldsymbol{v}(t) \equiv \dfrac{d\boldsymbol{r}(t)}{dt}$. Velocity is easily detectable with our natural senses since it is related with the change of pose of an object with respect to another object which serves as a reference frame. The acceleration vector $\boldsymbol{a}(t)$ is the rate of change of the velocity vector $\boldsymbol{v}(t)$ of the object over time. That is to say, $\boldsymbol{a}(t) \equiv \dfrac{d\boldsymbol{v}(t)}{dt} = \dfrac{d^2\boldsymbol{r}(t)}{dt^2}$. By resorting to Newton's second law, the acceleration can be interpreted as that which produces a static force as long as the moving object has mass and the acceleration remains

✉ Jaime GALLARDO-ALVARADO, email: jaime.gallardo@itcelaya.edu.mx
[1]National Technological Institute of Mexico, Celaya, Mexico.

constant. In this sense, acceleration analysis becomes important to determine the capacity of the servomotors employed in robot manipulators to move bodies.

The velocity and acceleration analyses are an ordinary task for most robot manipulators. However, nowadays robots need to operate at high speeds following smooth trajectories minimizing, among other benefits, the acceleration peaks and thus ameliorating the impulsive shaking forces, if any. In such a scenario, the velocity and acceleration analyses are insufficient to guarantee the optimal performance of such automated systems. The time derivative of the acceleration leads to the jerk $\boldsymbol{j}(t)$, i.e., $\boldsymbol{j}(t) \equiv \dfrac{d\boldsymbol{a}(t)}{dt} = \dfrac{d^3\boldsymbol{r}(t)}{dt^3}$, which by resorting to Newton's second law is understood as that which produces an impulsive force on an object as long as the jerk remains constant. The jerk has been the subject of in-depth studies with relevant applications such as curve smoothing, path planning trajectory, the modelling of superficial wear in cams, the evaluation of the performance of biomechanical systems, research on dynamical behavior of chaotic memory oscillators, multistable jerk chaotic systems, the perception of motion in living systems, and so on [1–12]. To have a simple idea of what jerk is consider that while velocity is clearly perceived when an object is moving and acceleration is perceived, for example, as a force that emerges when one is in a moving vehicle, the effects associated with the jerk are not consciously perceived. For example, the human body performs its movements minimizing the effects of jerk, a work that the brain performs automatically and instinctively. In this sense, it is worth mentioning that while the first serious studies on motion date from more than four centuries ago thanks to Galileo's contributions in the analysis of the motion of bodies in inclined planes, the study of jerk dates from less than half a century ago. This delay is perhaps because of the inherent difficulty of higher order derivatives when these are presented as simple derivatives product of a kind of blind mathematics lacking solid bases in the physical interpretation. For example, it is common in standard books on dynamics to explain the Coriolis acceleration in a few paragraphs and yet its extension to the Coriolis jerk can be somewhat obscure to the extent that the subject is simply excluded. On the other hand, the use of rational algebras that do not disregard physical sense, such as the screw theory, is essential for a comprehensive treatise on higher-order analysis of robotic systems. The usefulness is clear when, for example, in designing the Hubble space telescope, NASA set limits not only for the jerk but also for the jounce.

Fig. 1 shows the PUMA robot, undoubtedly the most famous serial manipulator in history. The PUMA robot marked the before and after of modern robotics. PUMA is the acronym for Programmable Universal Assembly Machine or Programmable Universal Manipulator Arm and was initially developed for General Motors thanks to the research work of Victor Scheinman sponsored by MIT and Stanford University. Subsequently, UNIMATION gave the final push for its inclusion in the industry. PUMA is an emblematic robot with which modern robotics manifested its intention to emulate the movement of the arms of the human body.

Fig. 1. The PUMA robot

Its potential was immediately recognized in the industry raising great expectations and quickly went from being an academic research to a real application.

In this work, the jerk analysis of the PUMA robot is approached by means of the screw theory. As an intermediate step, for the sake of completeness the velocity and acceleration analyses of the robot are also included. Numerical examples are included in order to illustrate the versatility of the kinematic analysis method employed.

2. Preliminaries

For non-experts in the subject, in this section fundamentals of Plücker coordinates and the theory of screws are briefly explained.

2.1. Plücker coordinates of lines

Plücker coordinates were introduced by Julius Plücker as a geometric tool to assign six homogeneous coordinates to each line in projective 3-space, $\mathbb{P}^3$. Plücker coordinates satisfy a quadratic constraint and therefore it is possible to establish a one-to-one correspondence between the 4-dimensional space of lines in $\mathbb{P}^3$ and points on a quadric in $\mathbb{P}^5$ (projective 5-space). They can be extended to coordinates for the screws and wrenches employed in screw theory to solve the kinematics and dynamics of robot manipulators.

Let ℓ be a line segment, see Fig. 2. The line ℓ is characterized by a defined number of parameters with which it is possible to differentiate it from other lines. The determination of the parameters associated with a line marks the beginning of the study of Plücker coordinates. To this end, let us consider that $\hat{\boldsymbol{\ell}}$ is a unit vector along the line ℓ while p is a point through which the line passes. Furthermore, let us consider that $\boldsymbol{p}$ is the position vector of point p. Hence, it is possible to define a moment vector $\boldsymbol{m}$ as $\boldsymbol{m} = \boldsymbol{p} \times \hat{\boldsymbol{\ell}}$. If we choose another point of the line, for example

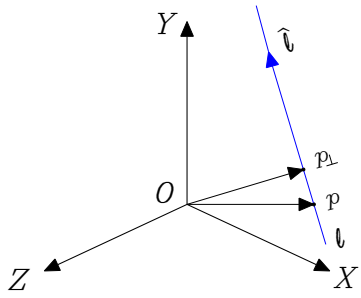

Fig. 2. A spatial line ℓ

$\bar{\boldsymbol{p}} = \boldsymbol{p} + \lambda\hat{\boldsymbol{\ell}}$ where $\lambda \in \mathbb{R}$, then the moment $\bar{\boldsymbol{m}}$ produced by $\bar{p}$ may be computed as

$$\bar{\boldsymbol{m}} = (\boldsymbol{p} + \lambda\hat{\boldsymbol{\ell}}) \times \hat{\boldsymbol{\ell}} = \boldsymbol{p} \times \hat{\boldsymbol{\ell}} + \lambda(\hat{\boldsymbol{\ell}} \times \hat{\boldsymbol{\ell}}) = \boldsymbol{p} \times \hat{\boldsymbol{\ell}}. \tag{1}$$

In other words, $\bar{\boldsymbol{m}} = \boldsymbol{m}$, which means that any point of the line segment produces the same moment about the point O. It is evident that the vectors $\hat{\boldsymbol{\ell}}$ and $\boldsymbol{m}$ provide complete data to characterize a line. In that concern, the Plücker coordinates of the line ℓ, notated as $\boldsymbol{L}$, are defined as the concatenation of the vectors $\hat{\boldsymbol{\ell}}$ and $\boldsymbol{m}$ as follows

$$\boldsymbol{L} = \begin{bmatrix} \hat{\boldsymbol{\ell}} \\ \boldsymbol{m} \end{bmatrix}. \tag{2}$$

Note that for the general case one would suppose the $\boldsymbol{L}$ must be a six-dimensional vector, a redundant assumption that contradicts the first paragraph of this section. To elucidate this point, let us consider that in geometry a line is an infinitely long object with no width, depth, or curvature. Thus, to determine the maximum dimension of $\boldsymbol{L}$ it is necessary to take into proper account two conditions:

1. The vectors $\boldsymbol{m}$ and $\hat{\boldsymbol{\ell}}$ are orthogonal. Therefore, we have a constraint equation given by $\boldsymbol{m} \cdot \hat{\boldsymbol{\ell}} = (\boldsymbol{p} \times \hat{\boldsymbol{\ell}}) \cdot \hat{\boldsymbol{\ell}} = 0$.
2. The vector $\hat{\boldsymbol{\ell}}$ is unitary. Thus, the second condition implies that $| \hat{\boldsymbol{\ell}} | = 1$.

Even though the correctness of these points, to achieve the compatibility between Plücker coordinates and the Lie algebra $se(3)$ of the Euclidean group $SE(3)$, it is necessary to keep the redundancy of the Plücker vector.

2.1.1. Reciprocal product between two lines

The reciprocal product between two lines is one of the highlights of Plücker coordinates. Referring Fig. 3, let us consider a line ℓ in space passing through point p. Furthermore, let q be an arbitrary point. The handling of points p and q yields interesting clues about the reciprocal product concept.

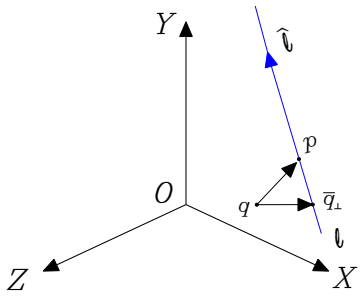

Fig. 3. A line ℓ in the space passing through point p

The moment vector $\boldsymbol{m}_q$ produced by the unit vector $\hat{\boldsymbol{\ell}}$ about point q may be computed as

$$\boldsymbol{m}_q = (\boldsymbol{p} - \boldsymbol{q}) \times \hat{\boldsymbol{\ell}}. \tag{3}$$

Thus

$$\boldsymbol{m}_q = \boldsymbol{m}_O - \boldsymbol{q} \times \hat{\boldsymbol{\ell}}, \tag{4}$$

where $\boldsymbol{m}_O = \boldsymbol{p} \times \hat{\boldsymbol{\ell}}$ is the moment produced by $\hat{\boldsymbol{\ell}}$ about the origin O of the reference frame O_XYZ. On the other hand, without loss of generality, one can choose a point $\bar{q}$ in such a way that the relative vector $\bar{\boldsymbol{q}} - \boldsymbol{q}$ is perpendicular to the line ℓ. Then, the vector $\boldsymbol{m}_q$ may be computed as

$$\boldsymbol{m}_q = (\bar{\boldsymbol{q}} - \boldsymbol{q}) \times \hat{\boldsymbol{\ell}}, \tag{5}$$

Pre-multiplying both sides of Eq. (5) by the vector $\hat{\boldsymbol{\ell}}$ it follows that

$$\hat{\boldsymbol{\ell}} \times \boldsymbol{m}_q = \hat{\boldsymbol{\ell}} \times ((\bar{\boldsymbol{q}} - \boldsymbol{q}) \times \hat{\boldsymbol{\ell}}). \tag{6}$$

However

$$\hat{\boldsymbol{\ell}} \times ((\bar{\boldsymbol{q}} - \boldsymbol{q}) \times \hat{\boldsymbol{\ell}}) = \hat{\boldsymbol{\ell}} \cdot \hat{\boldsymbol{\ell}}(\bar{\boldsymbol{q}} - \boldsymbol{q}) - \hat{\boldsymbol{\ell}} \cdot (\bar{\boldsymbol{q}} - \boldsymbol{q})\hat{\boldsymbol{\ell}}. \tag{7}$$

Hence

$$\hat{\boldsymbol{\ell}} \times \boldsymbol{m}_q = \bar{\boldsymbol{q}} - \boldsymbol{q}. \tag{8}$$

Which lead us

$$\bar{\boldsymbol{q}} = \boldsymbol{q} + \hat{\boldsymbol{\ell}} \times \boldsymbol{m}_q. \tag{9}$$

Gathering these results we are in a position to define the reciprocal product.

Theorem 1 *Let us consider that ℓ_1 and ℓ_2 are two lines whose Plücker coordinates, see Eq. (2), are given by*

$$\boldsymbol{L}_i = \begin{bmatrix} \hat{\boldsymbol{\ell}}_i \\ \boldsymbol{m}_i \end{bmatrix} \quad i = 1, 2. \tag{10}$$

The reciprocal product $(*)$ between $\boldsymbol{L}_1$ and $\boldsymbol{L}_2$ is given by

$$\boldsymbol{L}_1 * \boldsymbol{L}_2 \equiv \hat{\boldsymbol{\ell}}_1 \cdot \boldsymbol{m}_2 + \hat{\boldsymbol{\ell}}_2 \cdot \boldsymbol{m}_1. \tag{11}$$

Proof: according to Eq. (4), the vector $\boldsymbol{m}_1$ associated to the line ℓ_1 may be related with the vector $\boldsymbol{m}_2$ associated to the line ℓ_2 as follows

$$\boldsymbol{m}_1 = \boldsymbol{m}_2 - \boldsymbol{p}_1 \times \hat{\boldsymbol{\ell}}_2. \tag{12}$$

Furthermore, from the right side of Eq. (12) one can resort to the unit vector $\hat{\boldsymbol{\ell}}_1$ in such a way that

$$\hat{\boldsymbol{\ell}}_1 \cdot (\boldsymbol{m}_2 - \boldsymbol{p}_1 \times \hat{\boldsymbol{\ell}}_2) = \hat{\boldsymbol{\ell}}_1 \cdot \boldsymbol{m}_2 + \hat{\boldsymbol{\ell}}_2 \cdot (\boldsymbol{p}_1 \times \hat{\boldsymbol{\ell}}_1), \tag{13}$$

where evidently $\boldsymbol{p}_1 \times \hat{\boldsymbol{\ell}}_1 = \boldsymbol{m}_1$. Then, it follows that

$$\hat{\boldsymbol{\ell}}_1 \cdot (\boldsymbol{m}_2 - \boldsymbol{p}_1 \times \hat{\boldsymbol{\ell}}_2) = \hat{\boldsymbol{\ell}}_1 \cdot \boldsymbol{m}_2 + \hat{\boldsymbol{\ell}}_2 \cdot \boldsymbol{m}_1. \tag{14}$$

Finally, the left side of Eq. (14) is defined as the reciprocal product between the lines ℓ_1 and ℓ_2. That is to say, the reciprocal product is computed as

$$\boldsymbol{L}_1 * \boldsymbol{L}_2 \equiv \hat{\boldsymbol{\ell}}_1 \cdot \boldsymbol{m}_2 + \hat{\boldsymbol{\ell}}_2 \cdot \boldsymbol{m}_1. \tag{15}$$

and thus the proof is completed. □

Dealing with the instantaneous kinematics of robot manipulators, some relevant properties of the reciprocal product between two lines are as follows:

1. Assume that the lines ℓ_1 and ℓ_2 pass through a common point p. Then

$$\begin{aligned} \boldsymbol{L}_1 * \boldsymbol{L}_2 &= \hat{\boldsymbol{\ell}}_1 \cdot \boldsymbol{m}_2 + \hat{\boldsymbol{\ell}}_2 \cdot \boldsymbol{m}_1 \\ &= \hat{\boldsymbol{\ell}}_1 \cdot (\boldsymbol{p} \times \hat{\boldsymbol{\ell}}_2) + \hat{\boldsymbol{\ell}}_2 \cdot (\boldsymbol{p} \times \hat{\boldsymbol{\ell}}_1) \\ &= \hat{\boldsymbol{\ell}}_1 \cdot (\boldsymbol{p} \times \hat{\boldsymbol{\ell}}_2) - \hat{\boldsymbol{\ell}}_1 \cdot (\boldsymbol{p} \times \hat{\boldsymbol{\ell}}_2) = 0. \end{aligned}$$

2. Assume that the line ℓ_1 passes through point p while the line ℓ_2 passes through point q. If the lines are parallel then $\hat{\boldsymbol{\ell}}_1 = \hat{\boldsymbol{\ell}}_2 = \hat{\boldsymbol{\ell}}$. Therefore

$$\boldsymbol{L}_1 * \boldsymbol{L}_2 = \hat{\boldsymbol{\ell}} \cdot \boldsymbol{m}_2 + \hat{\boldsymbol{\ell}} \cdot \boldsymbol{m}_1 = \hat{\boldsymbol{\ell}} \cdot (\boldsymbol{q} \times \hat{\boldsymbol{\ell}}) + \hat{\boldsymbol{\ell}} \cdot (\boldsymbol{p} \times \hat{\boldsymbol{\ell}}) = 0.$$

3. If the unit vector $\hat{\boldsymbol{l}}_1$ vanishes and $\boldsymbol{m}_1 = \hat{\boldsymbol{l}}_2$ then we have that

$$\boldsymbol{L}_1 * \boldsymbol{L}_2 = \hat{\boldsymbol{\ell}}_1 \cdot \boldsymbol{m}_2 + \hat{\boldsymbol{\ell}}_2 \cdot \boldsymbol{m}_1 = \boldsymbol{0} \cdot \boldsymbol{m}_2 + \hat{\boldsymbol{\ell}}_2 \cdot \hat{\boldsymbol{\ell}}_2 = 0 + 1 = 1.$$

2.2. Fundamentals of screw theory

Chevallier [13] was the first to envision the infinitesimal motion of the rigid body as the geometrical representation of a field with helical properties. The importance of this postulate is extraordinary if one takes into account that the physical space E and the three dimensional vector space $\mathbb{R}^3$ are related by a helical vector field as follows

$$X : E \to \mathbb{R}^3 \quad X(P) = X(P) \forall P \in E, \tag{16}$$

where $X(P) \in \mathbb{R}^3$. Furthermore, given two points $P, Q \in E$ it follows that

$$X(Q) = X(P) + \boldsymbol{a} \times \boldsymbol{r}_{Q/P}\,, \tag{17}$$

where the vector $\boldsymbol{a}$ is the vector of the helical vector field while $\boldsymbol{r}_{Q/P}$ is the position vector of point Q with respect to point P.

2.2.1. Kinematic states of the rigid body

Fig. 4 shows a body m in motion with respect to another body j. Attached to body j there is a reference frame O_XYZ where the origin O plays the role of reference pole. Reference pole means that a point of the body m coincides instantaneously with the point O. From a kinematic point of view, in a mechanism the connection between its links is relevant but not their shape, so it is always possible to make a point of the link coincide instantaneously with the point O without affecting the infinitesimal kinematic analysis.

The instantaneous rotational motion of body m as measured from body j ranges from the angular velocity vector ${}^j\boldsymbol{\omega}^m$ to the angular jerk vector ${}^j\boldsymbol{\zeta}^m$ without overlooking, naturally, the angular acceleration vector ${}^j\boldsymbol{\alpha}^m$. These vectors do not

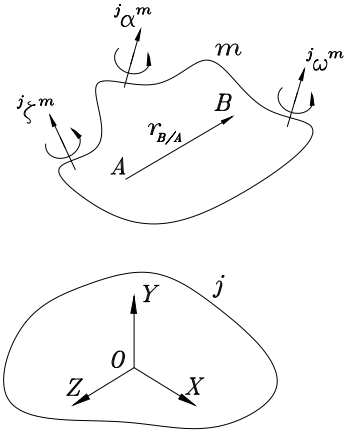

Fig. 4. Bodies m and j in relative motion

depend on any particular point embedded in the body m so they can be considered as properties of the rigid body. However, the angular properties of the rigid body alone are insufficient to fully characterize the motion of it. To overcome this point it is necessary to include the linear motion of the point of interest of the rigid body. A kinematic state is a vector entity that contains the complete information to determine the angular and linear kinematic quantities of any point of the moving body, of course at the desired level of the kinematic analysis. A kinematic state, notated as $\boldsymbol{M} = \begin{bmatrix} \boldsymbol{p}_* \\ \boldsymbol{d}_* \end{bmatrix}$, consists of a primal part $\boldsymbol{p}_*$ and a dual part $\boldsymbol{d}_*$. The primal part is devoted to the angular vector while the dual part is associated with the corresponding linear vector.

The first kinematic state to be explained is the velocity state of the rigid body, notated as ${}^j\boldsymbol{V}_Q^m$, also known as the twist about a screw, where Q is the point of interest of the rigid body. Ball [14] defined the velocity state of rigid body, see Fig. 4, as follows

$$ {}^j\boldsymbol{V}_Q^m = \begin{bmatrix} {}^j\boldsymbol{\omega}^m \\ \boldsymbol{v}_Q \end{bmatrix}, \tag{18} $$

where $\boldsymbol{v}_Q$ is the velocity vector of point Q. Expression (18) is the logical vector to define the velocity state. The correctness of this definition can be validated by resorting to the theory of helical fields. To this aim, let us consider two points A and B of body m. The velocity states of these bodies are given by

$$ {}^j\boldsymbol{V}_A^m = \begin{bmatrix} {}^j\boldsymbol{\omega}^m \\ \boldsymbol{v}_A \end{bmatrix}, \quad {}^j\boldsymbol{V}_B^m = \begin{bmatrix} {}^j\boldsymbol{\omega}^m \\ \boldsymbol{v}_B \end{bmatrix}. \tag{19} $$

Since the primal part of ${}^j\boldsymbol{V}_A^m$ and ${}^j\boldsymbol{V}_B^m$ is the same, then the first condition of a helical field is satisfied. On the other hand, by resorting to elementary kinematics, the velocity vector of point B may be computed upon the velocity vector of point A as follows

$$ \boldsymbol{v}_B = \boldsymbol{v}_A + {}^j\boldsymbol{\omega}^m \times \boldsymbol{r}_{B/A}\,, \tag{20} $$

where $\boldsymbol{r}_{B/A}$ is the relative position vector between B and A. Hence one obtains that

$$ \boldsymbol{d}_B = \boldsymbol{d}_A + {}^j\boldsymbol{\omega}^m \times \boldsymbol{r}_{B/A}\,, \tag{21} $$

and the second condition of a helical field is satisfied.

The next kinematic state to be considered is the acceleration state of rigid body. More than half a century ago, Brand [15] defined the acceleration state of rigid body as follows

$$ {}^j\boldsymbol{A}_Q^m = \begin{bmatrix} {}^j\boldsymbol{\alpha}^m \\ \boldsymbol{a}_Q - {}^j\boldsymbol{\omega}^m \times \boldsymbol{v}_Q \end{bmatrix}, \tag{22} $$

where ${}^j\boldsymbol{\alpha}^m = \dfrac{{}^j d\,{}^j\boldsymbol{\omega}^m}{dt}$ is the angular acceleration vector of body m as measured from body j while $\boldsymbol{a}_Q$ is the acceleration vector of point Q. At this point an elementary doubt arises, does Brand's definition of the acceleration state satisfy the helical vector field conditions? To answer this question let us consider the reduced acceleration states of points A and B. Indeed

$$ {}^j\boldsymbol{A}^m_A = \begin{bmatrix} {}^j\boldsymbol{\alpha}^m \\ \boldsymbol{a}_A - {}^j\boldsymbol{\omega}^m \times \boldsymbol{v}_A \end{bmatrix}, \quad {}^j\boldsymbol{A}^m_B = \begin{bmatrix} {}^j\boldsymbol{\alpha}^m \\ \boldsymbol{a}_B - {}^j\boldsymbol{\omega}^m \times \boldsymbol{v}_B \end{bmatrix}. \tag{23} $$

Clearly, the first condition of a helical field is satisfied, i.e., the primal part, or vector ${}^j\boldsymbol{\alpha}^m$, of both acceleration states is the same. To prove the second condition, by resorting to elementary kinematics we have that

$$ \boldsymbol{a}_B = \boldsymbol{a}_A + {}^j\boldsymbol{\omega}^m \times \boldsymbol{v}_{B/A} + {}^j\boldsymbol{\alpha}^m \times \boldsymbol{r}_{B/A}\,. \tag{24} $$

Hence

$$ \boldsymbol{a}_B = \boldsymbol{a}_A + {}^j\boldsymbol{\omega}^m \times (\boldsymbol{v}_B - \boldsymbol{v}_A) + {}^j\boldsymbol{\alpha}^m \times \boldsymbol{r}_{B/A} \tag{25} $$

or

$$ \boldsymbol{a}_B - {}^j\boldsymbol{\omega}^m \times \boldsymbol{v}_B = \boldsymbol{a}_A - {}^j\boldsymbol{\omega}^m \times \boldsymbol{v}_A + {}^j\boldsymbol{\alpha}^m \times \boldsymbol{r}_{B/A}\,. \tag{26} $$

Note that the left side of Eq. (26) is precisely the dual part of the acceleration state ${}^j\boldsymbol{A}^m_B$ while the right side is the dual part of the acceleration state ${}^j\boldsymbol{A}^m_A$ plus the cross product ${}^j\boldsymbol{\alpha}^m \times \boldsymbol{r}_{B/A}$. Furthermore, the vector ${}^j\boldsymbol{\alpha}^m$ is the primal part of both acceleration states. This confirms that Brand's definition of the acceleration state of rigid body satisfies the conditions of a helical field.

Finally, the jerk state of the body m as observed from the body j was formulated by Rico et al [16] as

$$ {}^j\boldsymbol{J}^m_Q = \begin{bmatrix} {}^j\boldsymbol{\zeta}^m \\ \boldsymbol{p}_Q - 2\,{}^j\boldsymbol{\alpha}^m \times \boldsymbol{v}_Q - {}^j\boldsymbol{\omega}^m \times \boldsymbol{a}_Q \end{bmatrix}, \tag{27} $$

where ${}^j\boldsymbol{\zeta}^m = \dfrac{{}^j d}{dt}\,{}^j\boldsymbol{\alpha}^m$ is the angular jerk vector of body m as measured from body j, while $\boldsymbol{p}_Q = \dfrac{{}^j d}{dt}\boldsymbol{a}_Q$ is the linear jerk vector of point Q. To prove the correctness of Eq. (27) let us consider that the jerk states of points A and B are given by

$$ {}^j\boldsymbol{J}^m_A = \begin{bmatrix} {}^j\boldsymbol{\zeta}^m \\ \boldsymbol{p}_A - 2\,{}^j\boldsymbol{\alpha}^m \times \boldsymbol{v}_A - {}^j\boldsymbol{\omega}^m \times \boldsymbol{a}_A \end{bmatrix}, \; {}^j\boldsymbol{J}^m_B = \begin{bmatrix} {}^j\boldsymbol{\zeta}^m \\ \boldsymbol{p}_B - 2\,{}^j\boldsymbol{\alpha}^m \times \boldsymbol{v}_B - {}^j\boldsymbol{\omega}^m \times \boldsymbol{a}_B \end{bmatrix}. \tag{28} $$

The first condition of a helical field is immediately satisfied, i.e., the primal part or vector ${}^{j}\boldsymbol{\zeta}^{m}$ of both jerk states is the same. On the other hand, the linear jerk vector of point B is computed upon the linear jerk vector of point A as follows

$$\boldsymbol{p}_B = \boldsymbol{p}_A - \boldsymbol{p}_{B/A}\,, \tag{29}$$

where, see refs. [16, 17], the relative jerk vector between points A and B is given by

$$\boldsymbol{p}_{B/A} = 2^{j}\boldsymbol{\alpha}^{m} \times \boldsymbol{v}_{B/A} + {}^{j}\boldsymbol{\omega}^{m} \times \boldsymbol{a}_{B/A} + {}^{j}\boldsymbol{\zeta}^{m} \times \boldsymbol{r}_{B/A}\,, \tag{30}$$

Thus, after a few computations it follows that

$$\boldsymbol{p}_B - 2^{j}\boldsymbol{\alpha}^{m} \times \boldsymbol{v}_B - {}^{j}\boldsymbol{\omega}^{m} \times \boldsymbol{a}_B = \boldsymbol{p}_A - 2^{j}\boldsymbol{\alpha}^{m} \times \boldsymbol{v}_A - {}^{j}\boldsymbol{\omega}^{m} \times \boldsymbol{a}_A + {}^{j}\boldsymbol{\zeta}^{m} \times \boldsymbol{r}_{B/A} \tag{31}$$

or

$$\boldsymbol{d}_B = \boldsymbol{d}_A + {}^{j}\boldsymbol{\zeta}^{m} \times \boldsymbol{r}_{B/A}\,. \tag{32}$$

and the conditions of a helical field for expression (27) are completed.

2.2.2. Screw theory and kinematic chains

In this part of the contribution, it is provided the relationship between the kinematic states of rigid body and the infinitesimal screws representing the kinematic pairs of a serial chain. For details of these concepts the reader is referred to [18].

A screw \$ is formed with two vectors $\hat{\boldsymbol{s}}$ and $\boldsymbol{s}_O$ where the unit vector $\hat{\boldsymbol{s}}$ is the direction of the axis of the screw, known as the Instantaneous Screw Axis (ISA), while $\boldsymbol{s}_O$ is the moment produced by $\hat{\boldsymbol{s}}$ about a point O named the reference pole. The vectors $\hat{\boldsymbol{s}}$ and $\boldsymbol{s}_O$ are designated, respectively, as the primal and dual parts of the screw. The moment $\boldsymbol{s}_O$ is computed using the pitch h of the screw as $\boldsymbol{s}_O = h\hat{\boldsymbol{s}} + \hat{\boldsymbol{s}} \times \boldsymbol{r}_O$ where $\boldsymbol{r}_O$ is a vector starting at an arbitrary point of the ISA and ending at the reference pole O. A screw splendidly confirms the celebrated Chasles theorem, which states that the spatial displacement of a rigid body can be represented by a rotation around an axis followed by a translation parallel to the same axis. Furthermore, since a screw bears a direct relationship to the Plücker coordinates of a line, then a set of complex lines is a set of lines whose Plücker coordinates satisfy a linear relationship which can be associated with the instantaneous motion of the rigid body.

Fig. 5 shows a kinematic chain serially connected by helical pairs which are notated as ${}^{k}\$^{k+1}\,(k = 0, 1, 2, \ldots, m-1)$. The fixed link is labelled as 0 while the end link is labelled as m.

The velocity state of the body m as observed from the body 0 can be written in terms of the infinitesimal screws associated with the kinematic pairs of the serial

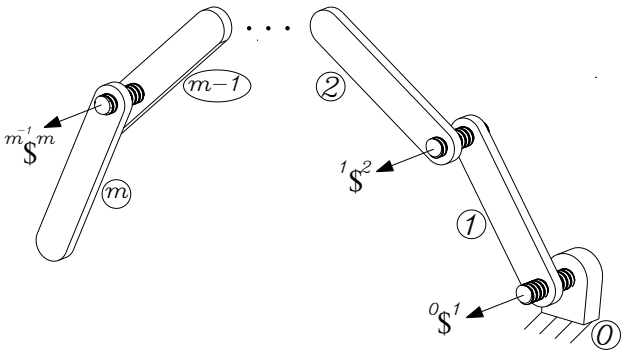

Fig. 5. Open kinematic chain and its infinitesimal screws

chain as follows [19]

$$ {}^{0}\boldsymbol{V}_{O}^{m} = \sum_{i=0}^{m-1} {}_{i}\omega_{i+1}\, {}^{i}\$^{i+1}, \tag{33} $$

where ${}_{i}\omega_{i+1} (i = 0, 1, \ldots, m-1)$ is the joint velocity rate between bodies $i+1$ and i. Expression (33) marks the successful beginning of the screw theory in the kinematic analysis of robotic manipulators. However, the extension of this expression to acceleration analysis was not as immediate as one might suppose. Thus, detractors of screw theory found for several decades arguments to discredit the value of this algebra and to pigeon-hole it as an academic curiosity of little use and forever limited to velocity analysis. It took several decades after the publication of Sugimoto and Duffy [19] for screw theory to finally emerge from its slumber and be properly extended to acceleration analysis of kinematic chains thanks to the work of Rico and Duffy [20]. After unfounded criticisms and some skepticism, the acceleration analysis of kinematic chains in screw form was finally formulated and accepted as

$$ {}^{0}\boldsymbol{A}_{O}^{m} = \sum_{i=0}^{m-1} {}_{i}\alpha_{i+1}\, {}^{i}\$^{i+1} + \$_{a}\,, \tag{34} $$

where ${}_{i}\alpha_{i+1} = \dfrac{d_i\omega_{i+1}}{dt}$ is the joint acceleration rate of body $i+1$ as observed from body i while $\$_a$ is designated as the Lie screw of acceleration, after Marius Sophus Lie, which is calculated as

$$ \$_{a} = \sum_{i=0}^{m-2} \left[{}_{i}\omega_{i+1}\, {}^{i}\$^{i+1} \quad \sum_{j=i+1}^{m-1} {}_{j}\omega_{j+1}\, {}^{j}\$^{j+1} \right], \tag{35} $$

where the brackets $\left[* \quad * \right]$ denote the Lie product, a fundamental operation of the Lie algebra $se(3)$ of the Euclidean group $SE(3)$. Note that the Lie screw of

acceleration is related with Coriolis terms. In that sense, it is somewhat strange to read that some authors conclude that by means of experiments it is verified that the Coriolis and centrifugal forces are negligible in the PUMA robot [21].

The clarity with which the expression (34) was developed soon allowed it to be extended to the jerk analysis. The jerk state of body m as measured from the base link 0, notated as ${}^0\boldsymbol{J}_O^m$, in screw form is given by [16]

$$ {}^0\boldsymbol{J}_O^m = \sum_{i=0}^{m-1} {}_i\zeta_{i+1}\, {}^i\$^{i+1} + \$_j \,, \tag{36} $$

where $\$_j$ is called the Lie screw of jerk which is calculated as

$$ \$_j = \sum_{i=0}^{m-2} \left(2 \left[{}^i\boldsymbol{V}_O^{i+1} \quad {}^{i+1}\boldsymbol{A}_O^m \right] + \left[{}^i\boldsymbol{A}_O^{i+1} \quad {}^{i+1}\boldsymbol{V}_O^m \right] + \left[{}^i\boldsymbol{V}_O^{i+1} \left[{}^i\boldsymbol{V}_O^{i+1} \quad {}^{i+1}\boldsymbol{V}_O^m \right] \right] \right) . \tag{37} $$

Naturally, the corresponding velocity and acceleration states are computed by resorting to Eq. (33) and Eq. (34). Finally, note that the computation of nested Lie products is an unavoidable task to obtain the six-dimensional vector $\$_j$.

3. Plücker coordinates and the Lie algebra $se(3)$ of the Euclidean group $SE(3)$

The Lie algebra $se(3)$ of the Euclidean group $SE(3)$ is directly related with the Plücker coordinates of lines which is evidenced in the infinitesimal kinematic analysis of robotic manipulators owing to its isomorphism with screw theory [22–24]. At a glance, this appears to be a contradiction to the results previously presented. For example, in the general case a line in Plücker coordinates consists of six components of which, as already shown, two are redundant while an infinitesimal screw necessarily requires two concatenated three-dimensional vectors. It is therefore necessary to clarify the compatibility between these concepts.

First, it is essential to maintain the redundancy of the Plücker vector to achieve compatibility between the involved algebras. Considering that one has some freedom in the choice of the vector $\boldsymbol{p}$, then without losing generality it is feasible to select the vector $\boldsymbol{p}$ in such a way that it is perpendicular to the unit vector $\hat{\boldsymbol{\ell}}$. In this way, the magnitude of the vector $\boldsymbol{p}$, notated as p, is the minimum distance between the straight line ℓ and the origin O. At this point an extremely interesting task arises which consists of determining the Plücker coordinates of the line such that p goes to infinity. With this in mind, let us consider that $\prod$ is the plane generated by the straight line ℓ and the vector $\boldsymbol{p}$ which of course includes the origin O of the reference frame. Note that as the straight line ℓ is farther from the origin O in the

plane, the vector $\boldsymbol{m}$ grows such that the Plücker coordinates can be expressed by resorting to the original vector $\boldsymbol{m}$ as

$$\boldsymbol{L} = \begin{bmatrix} \hat{\boldsymbol{\ell}} \\ t\boldsymbol{m} \end{bmatrix}, \tag{38}$$

where $t \in \mathbb{R}$ is a scalar that amplifies the vector $\boldsymbol{m}$, i.e., $t > 1$. Therefore, it is possible to write a scaled Plücker vector $\boldsymbol{L}_s$ of $\boldsymbol{L}$ as

$$\boldsymbol{L}_s = \boldsymbol{L}/t = \begin{bmatrix} \hat{\boldsymbol{\ell}}/t \\ \boldsymbol{m} \end{bmatrix}. \tag{39}$$

Afterwards, if $t \to \infty$ then it follows that

$$\boldsymbol{L}_s = \lim_{t\to\infty} \begin{bmatrix} \hat{\boldsymbol{\ell}}/t \\ \boldsymbol{m} \end{bmatrix} = \begin{bmatrix} \lim\limits_{t\to\infty} \hat{\boldsymbol{\ell}}/t \\ \lim\limits_{t\to\infty} \boldsymbol{m} \end{bmatrix} = \begin{bmatrix} \boldsymbol{0} \\ \boldsymbol{m} \end{bmatrix}. \tag{40}$$

4. Higher-order kinematic analyses of the PUMA robot

This section focuses on the infinitesimal kinematic analysis, up to the jerk analysis, of the PUMA robot. In that sense, although the position analysis of the PUMA robot has been widely studied in previous works, see for instance [25–28], it is included in the contribution only for the sake of completeness of the section.

4.1. Position

The position analysis is addressed using the Denavit-Hartenberg convention, a classical method [29, 30]. Fig. 6 shows the topology of the PUMA robot, its parameters as well as its generalized coordinates $q_i (i = 1, 2, 3, \ldots, 6)$. Following the order $q_i (i = 1, 2, 3, \ldots, 6)$, the generalized coordinates are designated as waist, shoulder rotation, elbow, wrist rotation, wrist bend, and flange. Clearly, the solution of the position analysis requires six reference frames due to the constitutive elements of the six-degrees-of-freedom robot arm.

The end-effector, link 6, of the PUMA robot is related with the base link 0 through the homogeneous coordinates transformation matrix ${}^0\mathrm{T}^6 \in SE(3)$ as follows

$${}^0\mathrm{T}^6 = {}^0\mathrm{T}^1 \, {}^1\mathrm{T}^2 \, {}^2\mathrm{T}^3 \, {}^3\mathrm{T}^4 \, {}^4\mathrm{T}^5 \, {}^5\mathrm{T}^6, \tag{41}$$

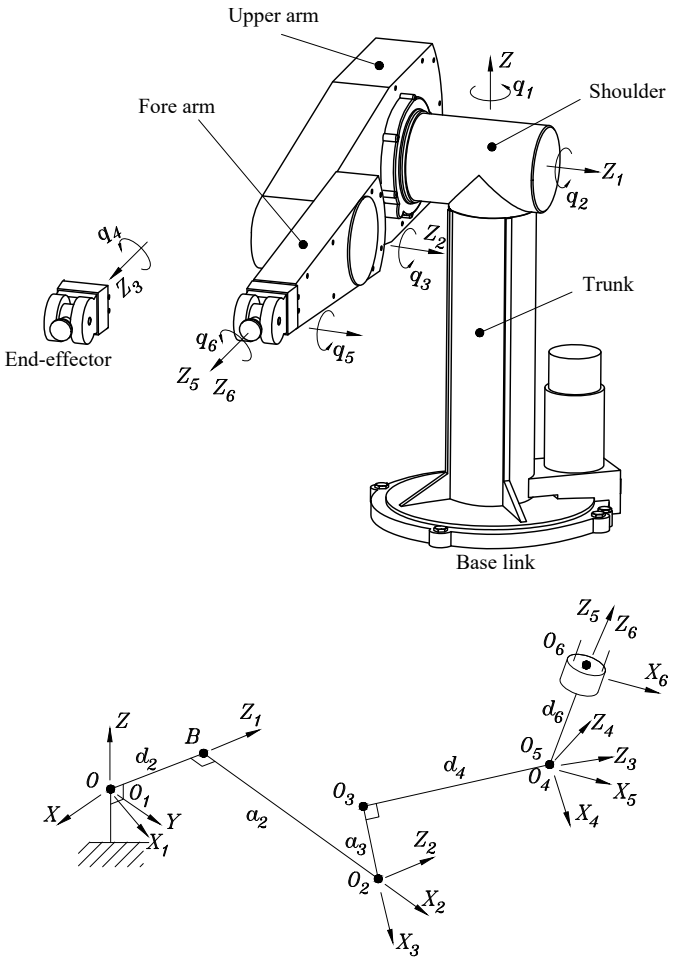

Fig. 6. The PUMA robot and its skeleton

where

$$ {}^0\mathrm{T}^1 = \begin{bmatrix} \cos q_1 & 0 & -\sin q_1 & 0 \\ \sin q_1 & 0 & \cos q_1 & 0 \\ 0 & -1 & 0 & 0 \\ 0 & 0 & 0 & 1 \end{bmatrix}, \quad {}^1\mathrm{T}^2 = \begin{bmatrix} \cos q_2 & -\sin q_2 & 0 & a_2 \cos q_2 \\ \sin q_2 & \cos q_2 & 0 & a_2 \sin q_2 \\ 0 & 0 & 1 & d_2 \\ 0 & 0 & 0 & 1 \end{bmatrix}, $$

$$ {}^2\mathrm{T}^3 = \begin{bmatrix} \cos q_3 & 0 & \sin q_3 & a_3 \cos q_3 \\ \sin q_3 & 0 & -\cos q_3 & a_3 \sin q_3 \\ 0 & 1 & 0 & 0 \\ 0 & 0 & 0 & 1 \end{bmatrix}, \quad {}^3\mathrm{T}^4 = \begin{bmatrix} \cos q_4 & 0 & -\sin q_4 & 0 \\ \sin q_4 & 0 & \cos q_4 & 0 \\ 0 & -1 & 0 & d_4 \\ 0 & 0 & 0 & 1 \end{bmatrix}, $$

$$ {}^4\mathrm{T}^5 = \begin{bmatrix} \cos q_5 & 0 & \sin q_5 & 0 \\ \sin q_5 & 0 & -\cos q_5 & 0 \\ 0 & 1 & 0 & 0 \\ 0 & 0 & 0 & 1 \end{bmatrix}, \quad {}^5\mathrm{T}^6 = \begin{bmatrix} \cos q_6 & -\sin q_6 & 0 & 0 \\ \sin q_6 & \cos q_6 & 0 & 0 \\ 0 & 0 & 1 & d_6 \\ 0 & 0 & 0 & 1 \end{bmatrix}. $$

Expression (41) may be employed to solving both, the inverse and the forward displacement analyses of the PUMA robot. In that concern, unlike the forward position analysis, the inverse position analysis is a challenging task that has been, however, successfully elucidated since several decades ago, see for instance [31–36]. Furthermore, it is worth to say that the inverse position analysis of 6R serial manipulators has been improved in recent years by resorting to the Dixon elimination method [37].

In the contribution, the position analysis focuses on the forward analysis. That is, given the generalized coordinates $q_i (i = 1, 2, 3, \ldots, 6)$ of the PUMA robot, it is necessary to determine the pose, position and orientation, of the end-effector. In short, it is required to determine the matrix ${}^0\mathrm{T}^6$ according to Eq. (41). Afterwards, assuming that P is a point of the end-effector, then the coordinates of $P = (X_P, Y_P, Z_P)$, expressed in the fixed reference frame, are obtained upon the relationship

$$ \begin{bmatrix} X_P \\ Y_P \\ Z_P \\ 1 \end{bmatrix} = {}^0\mathrm{T}^6 \begin{bmatrix} x_P \\ y_P \\ z_p \\ 1 \end{bmatrix}, \tag{42} $$

where (x_P, y_P, z_P) are the coordinates of P expressed in the moving reference frame $O_6X_6Y_6Z_6$.

4.2. Infinitesimal kinematics

To approach the infinitesimal kinematics of the PUMA robot, Fig. 7 shows the infinitesimal screws of the serial manipulator.

The equation of velocity in screw form of the PUMA robot is obtained by applying Eq. (33) using point O_6 as the reference pole as follows

$$ {}_0\omega_1\,{}^0\$^1 + {}_1\omega_2\,{}^1\$^2 + {}_2\omega_3\,{}^2\$^3 + {}_3\omega_4\,{}^3\$^4 + {}_4\omega_5\,{}^4\$^5 + {}_5\omega_6\,{}^5\$^6 = {}^0\boldsymbol{V}^6_{O_6}. \tag{43} $$

Taking into account that all the revolute joints of the PUMA robot are actuated then it follows that

$$ \dot{q}_1 = {}_0\omega_1, \quad \dot{q}_2 = {}_1\omega_2, \quad \dot{q}_3 = {}_2\omega_3, \quad \dot{q}_4 = {}_3\omega_4, \quad \dot{q}_5 = {}_4\omega_5, \quad \dot{q}_6 = {}_5\omega_6. $$

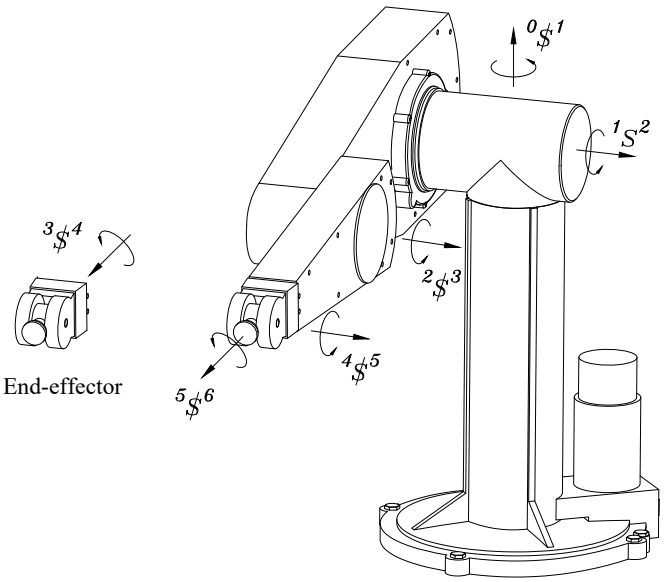

Fig. 7. Infinitesimal screws of the PUMA robot

By arranging in matrix form expression (43), the input-output equation of velocity of the manipulator is compactly obtained as

$$\mathrm{J}\,\mathrm{Q_v} = \mathrm{I_6}\,{}^0\boldsymbol{V}^6_{O_6}\,, \tag{44}$$

where J is the Jacobian matrix of the robot which is given by

$$\mathrm{J} = \left[{}^0\$^1 \quad {}^1\$^2 \quad {}^2\$^3 \quad {}^3\$^4 \quad {}^4\$^5 \quad {}^5\$^6\right], \tag{45}$$

whereas

$$\mathrm{Q_v} = \left[\dot{q}_1 \quad \dot{q}_2 \quad \dot{q}_3 \quad \dot{q}_4 \quad \dot{q}_5 \quad \dot{q}_6\right]^T \tag{46}$$

is the first-order driver matrix of the robot. Furthermore, $\mathrm{I_6}$ is the identity matrix of order 6.

Expression (44) allows for two types of velocity analysis. The first one is called the forward velocity analysis of the robot and consists of determining the velocity state ${}^0\boldsymbol{V}^6_O$ as long as the matrix $\mathrm{Q_v}$ is given. That is to say, assuming that the manipulator is in a defined reference configuration, when the revolute joints are actuated according to a set of generalized velocities $\dot{q}_i (i = 1, 2, 3, \ldots, 6)$ then the end-effector undergoes a velocity state ${}^0\boldsymbol{V}^6_O$. Excluding structural singularities credited to the position analysis, there are no restrictions for the computation of the velocity state ${}^0\boldsymbol{V}^6_O$. That is to say, the PUMA robot is free of

direct singularities. The second kind of velocity analysis is called the inverse velocity analysis of the robot and consists of computing the matrix Q_v to meet a desired velocity state ${}^0\boldsymbol{V}_O^6$. This analysis requires that the Jacobian matrix J must be invertible otherwise the robot manipulator is at a singular posture. Unlike the forward singularity, the inverse singularity is a reality and can be a serious problem for the performance of the PUMA robot. For example, if ${}^3\$^4 = {}^5\$^6$, see Fig. 7, then the screws of matrix J are linearly dependent causing that $\det(J) = 0$, and the robot manipulator evidently is at an inverse singularity. It is straightforward to demonstrate that actuating the revolute joint with the screw ${}^3\$^4$, the robot PUMA can escape from this particular example, for details the reader is referred to [38]. In short, the PUMA robot is incapable of executing arbitrary velocity states.

Once the velocity analysis was solved, the input-output equation of acceleration of the PUMA robot by applying Eq. (34) results in

$$\mathrm{J}\,\mathrm{Q_a} + \$a = {}^0\boldsymbol{A}_{O_6}^6\,, \tag{47}$$

where $\mathrm{Q_a} = \left[\ddot{q}_1 \quad \ddot{q}_2 \quad \ddot{q}_3 \quad \ddot{q}_4 \quad \ddot{q}_5 \quad \ddot{q}_6\right]^T$ is the second-order driver matrix of the PUMA robot while the Lie screw of acceleration $\$_a$ is computed as

$$\begin{aligned}\$a = &\left[\dot{q}_1\,{}^0\$^1 \quad \dot{q}_2\,{}^1\$^2 + \dot{q}_3\,{}^2\$^3 + \dot{q}_4\,{}^3\$^4 + \dot{q}_5\,{}^4\$^5 + \dot{q}_6\,{}^5\$^6\right] + \\ &\left[\dot{q}_2\,{}^1\$^2 \quad \dot{q}_3\,{}^2\$^3 + \dot{q}_4\,{}^3\$^4 + \dot{q}_5\,{}^4\$^5 + \dot{q}_6\,{}^5\$^6\right] + \\ &\left[\dot{q}_3\,{}^2\$^3 \quad \dot{q}_4\,{}^3\$^4 + \dot{q}_5\,{}^4\$^5 + \dot{q}_6\,{}^5\$^6\right] + \\ &\left[\dot{q}_4\,{}^3\$^4 \quad \dot{q}_5\,{}^4\$^5 + \dot{q}_6\,{}^5\$^6\right] + \left[\dot{q}_5\,{}^4\$^5 \quad \dot{q}_6\,{}^5\$^6\right].\end{aligned}$$

Finally, by resorting to expression (36), the input-output equation of jerk of the PUMA robot results in

$$\mathrm{J}\,\mathrm{Q_j} + \$_j = \boldsymbol{J}_{O_6}\,, \tag{48}$$

where $\mathrm{Q_j} = \left[\dddot{q}_1 \quad \dddot{q}_2 \quad \dddot{q}_3 \quad \dddot{q}_4 \quad \dddot{q}_5 \quad \dddot{q}_6\right]^T$ is the third-order driver matrix of the PUMA robot while the Lie screw of jerk $\$_j$ is given by

$$
\begin{aligned}
\$_j = {} & 2\Big[\dot{q}_1{}^0\$^1 \quad \ddot{q}_2{}^1\$^2 + \cdots + \ddot{q}_6{}^5\$^6 + [\dot{q}_3{}^2\$^3 \quad \dot{q}_4{}^3\$^4 + \cdots + \dot{q}_6{}^5\$^6] \\
& + \cdots + [\dot{q}_5{}^4\$^5 \quad \dot{q}_6{}^5\$^6]\Big] \\
& + 2\Big[\dot{q}_2{}^1\$^2 \quad \ddot{q}_3{}^2\$^3 + \cdots + \ddot{q}_6{}^5\$^6 + [\dot{q}_4{}^3\$^4 \quad \dot{q}_5{}^4\$^5 + \dot{q}_6{}^5\$^6] \\
& + [\dot{q}_5{}^4\$^5 \quad \dot{q}_6{}^5\$^6]\Big] + \cdots + 2\Big[\dot{q}_5{}^4\$^5 \quad \ddot{q}_6{}^5\$^6\Big] \\
& + \Big[\ddot{q}_1{}^0\$^1 \quad \dot{q}_2{}^1\$^2 + \cdots + \dot{q}_6{}^5\$^6\Big] + \Big[\ddot{q}_2{}^1\$^2 \quad \dot{q}_3{}^2\$^3 + \cdots + \dot{q}_6{}^5\$^6\Big] \\
& + \cdots + \Big[\ddot{q}_5{}^4\$^5 \quad \dot{q}_6{}^5\$^6\Big] \\
& + \Big[\dot{q}_1{}^0\$^1 \quad [\dot{q}_1{}^0\$^1 \quad \dot{q}_2{}^1\$^2 + \cdots + \dot{q}_6{}^5\$^6]\Big] \\
& + \Big[\dot{q}_2{}^1\$^2 \quad [\dot{q}_2{}^1\$^2 \quad \dot{q}_3{}^3\$^4 + \cdots + \dot{q}_6{}^5\$^6]\Big] \\
& + \cdots + \Big[\dot{q}_5{}^4\$^5 \quad [\dot{q}_5{}^4\$^5 \quad \dot{q}_6{}^5\$^6]\Big].
\end{aligned}
$$

Finally, the jerk analysis of robot manipulators is not a trivial task. For example, this analysis is useful in the time optimal and jerk optimal for the manipulators in the presence of obstacles [39].

5. Simulation results

In this section, the equations of the instantaneous kinematics obtained by resorting to the theory of screws for the PUMA robot are applied in two numerical examples. Naturally, as an intermediate step, the displacement analysis is also addressed. The first example is focused on determining the conditions of position, velocity and acceleration of the robot so that from its reference configuration it reaches a given pose of the end-effector under specific conditions of motion both at the beginning and at the end of the motion. Example 2 is devoted to the computation of the temporal behavior of the jerk of the end-effector satisfying motion conditions imposed to the six active revolute joints of the robot or generalized coordinates. The numerical results of example 2 are validated using an alternative approach such as the implementation of algorithms based on sequential time derivatives of the analytic functions describing the displacement of the end-effector. To solve the numerical examples, let us consider that typical values for the Denavit-Hartenberg

parameters of the PUMA robot are as follows

$$a_2 = 431.8 \text{ [mm]}, \quad a_3 = -20.32 \text{ [mm]},$$
$$d_2 = 144.09 \text{ [mm]}, \quad d_4 = 433.07 \text{ [mm]}, \quad d_6 = 56.25 \text{ [mm]}.$$

Furthermore, let us consider that in the reference configuration of the robot the generalized coordinates are given by

$$q_1 = 0.2 \text{ [rad]}, \quad q_2 = 0.15 \text{ [rad]}, \quad q_3 = 0.25 \text{ [rad]},$$
$$q_4 = 0.3 \text{ [rad]}, \quad q_5 = 0.1 \text{ [rad]}, \quad q_6 = 0.25 \text{ [rad]}.$$

Of course, these data apply to both examples.

5.1. Example 1

The first example is devoted to perform numerically the time history of the velocity and acceleration analyses of the PUMA robot, focusing on the behavior of the end-effector as observed from the base link. For this purpose, consider that the manipulator starts from rest, both in velocity and acceleration, and after 4 seconds the robot returns to rest in such a way that the configuration of the robot meets the following generalized coordinates

$$q_1 = -0.5 \text{ [rad]}, \quad q_2 = 0.7 \text{ [rad]}, \quad q_3 = 0.4 \text{ [rad]},$$
$$q_4 = -0.8 \text{ [rad]}, \quad q_5 = 0.5 \text{ [rad]}, \quad q_6 = -0.7 \text{ [rad]}.$$

There is a considerable number of mathematical methods with which it is possible to achieve the desired conditions for the higher-order analysis, for instance by using complex methods such as cubic NURBS, fifth-order B-spline, the combination of the third-order spline with the septuple B-spline in the joint space to generate time-optimal and jerk-continuous trajectories, the time-optimal Acc/Dec method for multiple segments, and so on. An effective and simple option to meet the condition motions of example 1 is the use of fifth-order polynomial equations for the generalized coordinates [40]. This choice implies that six constraints are introduced for each active joint of the robot but fortunately in this part of the analysis we resort to the solution of simple linear equations. After a few computations, the functions of the generalized coordinates meeting the conditions imposed to the PUMA robot result to be the following univariate polynomial equations

$$\begin{aligned}
q_1 &= 0.2 - .109375t^3 + 0.410156250e - 1t^4 - 0.41015625e - 2t^5, \\
q_2 &= 0.15 + 0.859375e - 1t^3 - 0.322265625e - 1t^4 + 0.322265e - 2t^5, \\
q_3 &= 0.25 + 0.234375e - 1t^3 - 0.87890625e - 2t^4 + 0.8789062e - 3t^5, \\
q_4 &= 0.3 - .171875t^3 + 0.64453125e - 1t^4 - 0.64453125e - 2t^5, \\
q_5 &= 0.1 + 0.625e - 1t^3 - 0.234375e - 1t^4 + 0.234375e - 2t^5, \\
q_6 &= 0.25 - .1484375t^3 + 0.556640625e - 1t^4 - 0.556640625e - 2t^5,
\end{aligned} \tag{49}$$

where the time t is given in the interval $0 \leq t \leq 4$ [s]. Note that in this example, several coefficients of the univariate polynomial expressions (49) vanish, more specifically the coefficients of t and t^2. For clarity, Fig. 8 shows plots of functions (49) and their time derivatives. In the rest of the contribution, Maple sheets are used to generate the necessary plots.

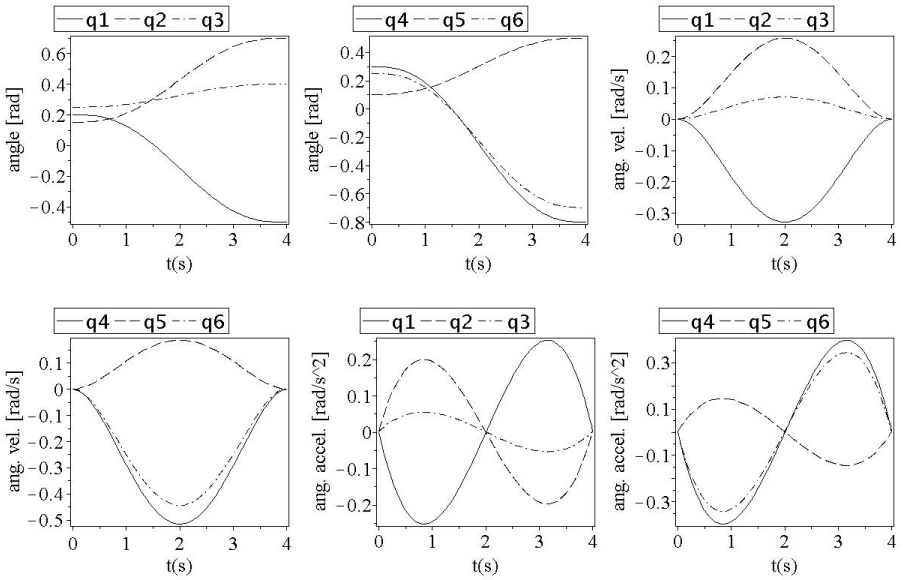

Fig. 8. Time history of the kinematics of the generalized coordinates of example 1

The time history of the coordinates of point O_6 expressed in the fixed reference frame O_XYZ by applying the Denavit-Hartenberg formulation is provided in Fig. 9.

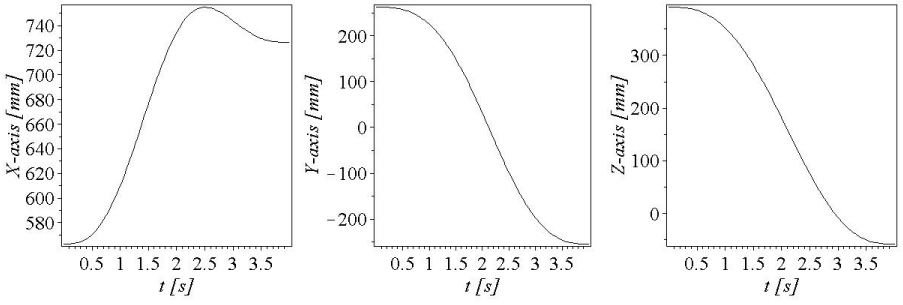

Fig. 9. Time history of the coordinates of point O_6 of example 1

The time history of the instantaneous kinematics of the end-effector of the PUMA robot by applying the theory of screws is provided in Fig. 10. In that

concern, the linear velocity and acceleration are computed for point O_6 of the end-effector.

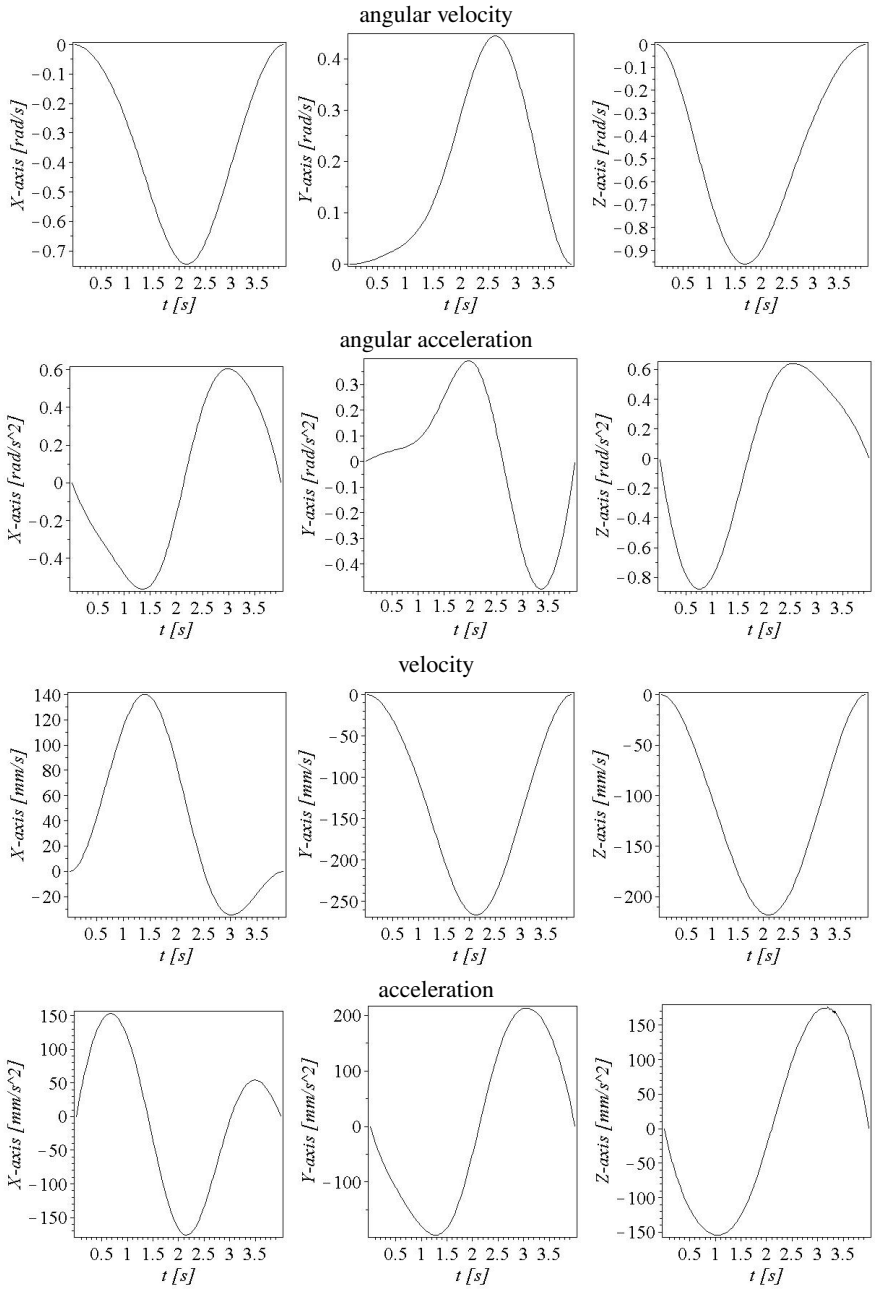

Fig. 10. Time history of the kinematics of the end-effector, example 1

As expected, the end-effector starts from rest and after the assigned time returns to rest by adopting the selected pose.

5.2. Example 2

To give an example for the computation of the jerk, in this subsection the numerical application is formulated as follows. Upon the reference configuration of the robot, the generalized coordinates are commanded to follow periodical functions given by

$$q_i(t) = q_i + \delta_i \sin t \cos t \quad i = 1 \sim 6, \tag{50}$$

where the time t is given in the interval $0 \leq t \leq 2\pi$ [s]. Furthermore, we have that

$$\delta_1 = 0.2 \text{ [rad]}, \quad \delta_2 = -0.15 \text{ [rad]}, \quad \delta_3 = -0.175 \text{ [rad]},$$
$$\delta_4 = 0.25 \text{ [rad]}, \quad \delta_5 = 0.15 \text{ [rad]}, \quad \delta_6 = -0.1 \text{ [rad]},$$

with these data it is required to compute the time history of the jerk of the end-effector as observed from the base link. Naturally, as intermediate steps, it is necessary to perform the position, velocity and acceleration analyses of the PUMA robot. Dealing with the linear components, point O_6 is chosen as the reference pole.

The time history of the coordinates of point O_6 expressed in the fixed reference frame O_XYZ by applying the Denavit-Hartenberg formulation is provided in Fig. 11.

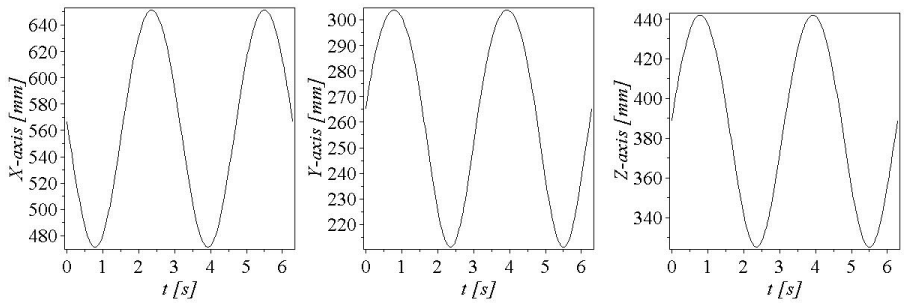

Fig. 11. Time history of the coordinates of point O_6, example 2

Afterwards, the application of the methodology of kinematic analysis developed in the contribution yields the time history of the angular infinitesimal kinematics of the end-effector provided in Fig. 12.

Furthermore, the time history of the linear components of velocity and acceleration for point O_6 of the end-effector is displayed in Fig. 13 while the time history of the jerk is reported in Fig. 15.

The validation of the results of example 2 by applying an alternative method is the next logical step.

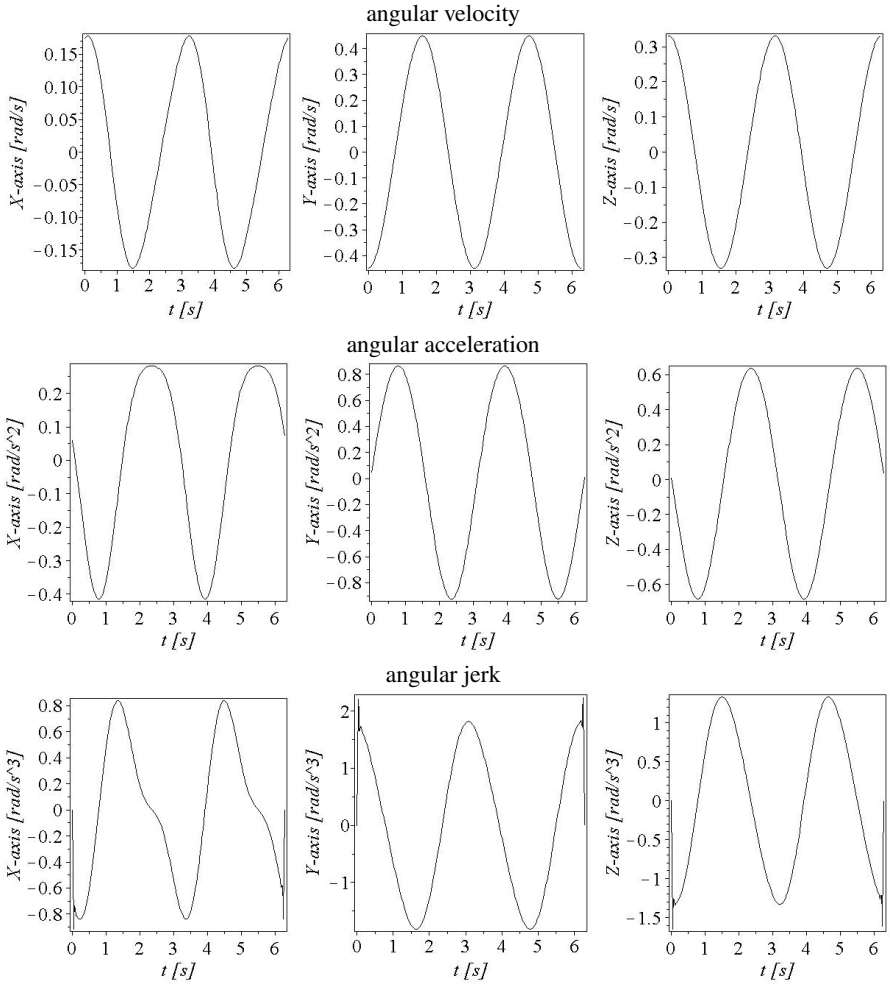

Fig. 12. Time history of the angular instantaneous kinematics of the end-effector, example 2

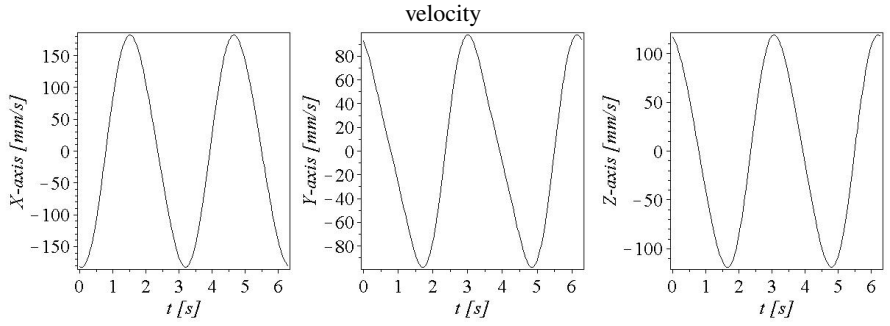

Fig. 13. Time history of the linear components of velocity and acceleration for point O_6, example 2

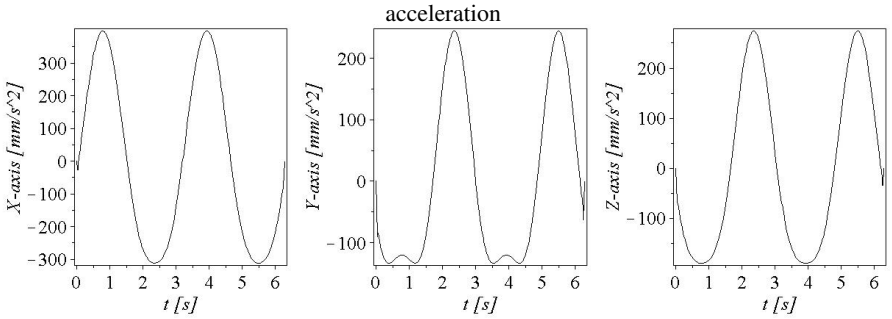

Fig. 13. cont. Time history of the linear components of velocity and acceleration for point O_6, example 2

5.3. Verification of numerical results

Due to the lack of a physical prototype, the strategy selected to verify the correctness of the numerical examples focuses on the calculation of the trajectory generated by the O_6 point of the end-effector using the Denavit-Hartenberg formulation and subsequently deriving such functions, which evidently depend on time, up to the third derivative. On the other hand, example 2 is the case selected for the validation of the results since validating both examples would only lead to a duplication of information. With this in mind, the coordinates of point $O_6 = (X(t), Y(t), Z(t))$, after applying the Denavit-Hartenberg formulation, result to be

$$\begin{aligned}
X(t) = {} & 56.25\big[\sin(.2+.2sc)\cos(.3+.25sc)\cos(.2+.2sc)\\
& \cos(-.15+.15sc)\cos(-.25+.175sc)\big]\\
& -56.25\big[\sin(.2+.2sc)\cos(.3+.25sc)\cos(.2+.2sc)\\
& \sin(-.15+.15sc)\sin(-.25+.175sc)\big]\\
& -56.25\cos^2(.2+.2sc)\cos(-.15+.15sc)\sin(-.25+.175sc)\\
& -56.25\cos^2(.2+.2sc)\sin(-.15+.15sc)\cos(-.25+.175sc)\\
& -433.07\cos(.2+.2sc)\cos(-.15+.15sc)\sin(-.25+.175sc)\\
& -433.07\cos(.2+.2sc)\sin(-.15+.15sc)\cos(-.25+.175sc)\\
& -20.32\cos(.2+.2sc)\cos(-.15+.15sc)\cos(-.25+.175sc)\\
& +20.32\cos(.2+.2sc)\sin(-.15+.15sc)\sin(-.25+.175sc)\\
& +431.8\cos(.2+.2sc)\cos(-.15+.15sc)\\
& +56.25\sin(.3+.25sc)\cos^2(.2+.2sc)\\
& -56.25\sin(.3+.25sc)-144.09\sin(.2+.2sc)
\end{aligned} \tag{51}$$

$$
\begin{aligned}
Y(t) = {} & 56.25\cos(.3+.25sc)\cos(-.15+.15sc)\cos(-.25+.175sc) \\
& -56.25\cos(.3+.25sc)\cos(-.15+.15sc)\cos(-.25+.175sc)\cos^2(.2+.2sc) \\
& -56.25\cos(.3+.25sc)\sin(-.15+.15sc)\sin(-.25+.175sc) \\
& +56.25\cos(.3+.25sc)\sin(-.15+.15sc)\sin(-.25+.175sc)\cos^2(.2+.2sc) \\
& +56.25\sin(.2+.2sc)\cos(.2+.2sc)\sin(.3+.25sc) \\
& -56.25\cos(.2+.2sc)\sin(.2+.2sc)\cos(-.15+.15sc)\sin(-.25+.175sc) \\
& -56.25\cos(.2+.2sc)\sin(.2+.2sc)\sin(-.15+.15sc)\cos(-.25+.175sc) \\
& -433.07\sin(.2+.2sc)\cos(-.15+.15sc)\sin(-.25+.175sc) \\
& -433.07\sin(.2+.2sc)\sin(-.15+.15sc)\cos(-.25+.175sc) \\
& -20.32\sin(.2+.2sc)\cos(-.15+.15sc)\cos(-.25+.175sc) \\
& +20.32\sin(.2+.2sc)\sin(-.15+.15sc)\sin(-.25+.175sc) \\
& +431.8\sin(.2+.2sc)\cos(-.15+.15sc)+144.09\cos(.2+.2sc)
\end{aligned}
\tag{52}
$$

$$
\begin{aligned}
Z(t) = {} & 56.25\cos(.3+.25sc)\sin(.2+.2sc)\sin(-.15+.15sc)\cos(-.25+.175sc) \\
& +56.25\cos(.3+.25sc)\sin(.2+.2sc)\cos(-.15+.15sc)\sin(-.25+.175sc) \\
& -56.25\cos(.2+.2sc)\sin(-.15+.15sc)\sin(-.25+.175sc) \\
& +56.25\cos(.2+.2sc)\cos(-.15+.15sc)\cos(-.25+.175sc) \\
& -433.07\sin(-.15+.15sc)\sin(-.25+.175sc) \\
& +433.07\cos(-.15+.15sc)\cos(-.25+.175sc) \\
& -20.32\sin(-.15+.15sc)\cos(-.25+.175sc) \\
& -20.32\cos(-.15+.15sc)\sin(-.25+.175sc) \\
& +431.8\sin(-.15+.15sc)
\end{aligned}
\tag{53}
$$

where $sc = \sin t \cos t$.

The velocity, acceleration and jerk of point O_6 are computed by sequentially applying the corresponding time derivatives to Eqs. (51)-(53). The generated plots up to the acceleration analysis of example 2 are reported in Fig. 14.

Please note that the plots of Fig. 14 are in excellent agreement with the plots of Figs. 11 and 13. After successful comparison of numerical results applying two different methods, the jerk of point O_6 is provided in Fig. 15.

Finally, it is noteworthy how the numerical results of the jerk analysis using screw theory agree reasonably well with those obtained when using an alternative method such as the direct application of time derivatives to analytic functions associated with the robot position analysis. Even though the same results are obtained, it is important to point out that when the screw theory is applied, the

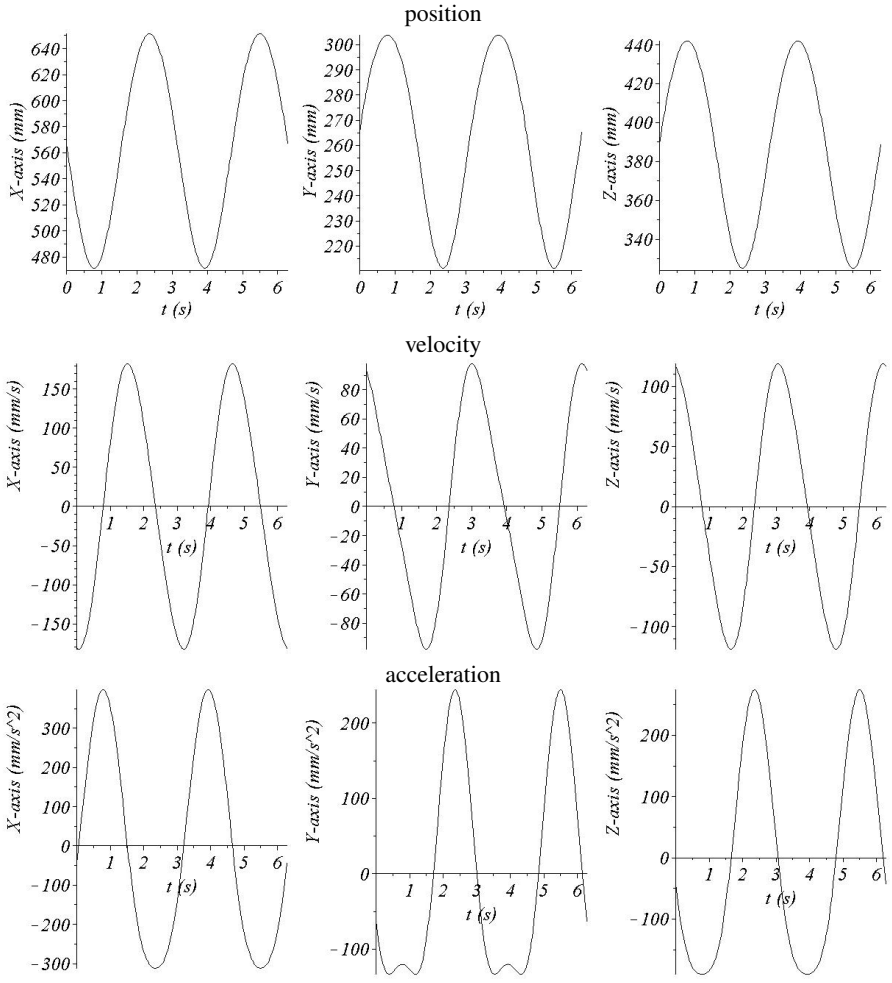

Fig. 14. Time history of the kinematics of point O_6 up to the acceleration analysis using time derivatives of analytic functions. Example 2

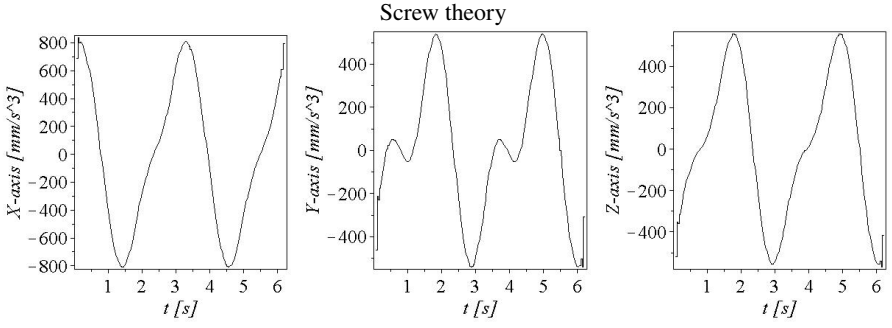

Fig. 15. Time history of the jerk of point O_6 using two different methods. Example 2

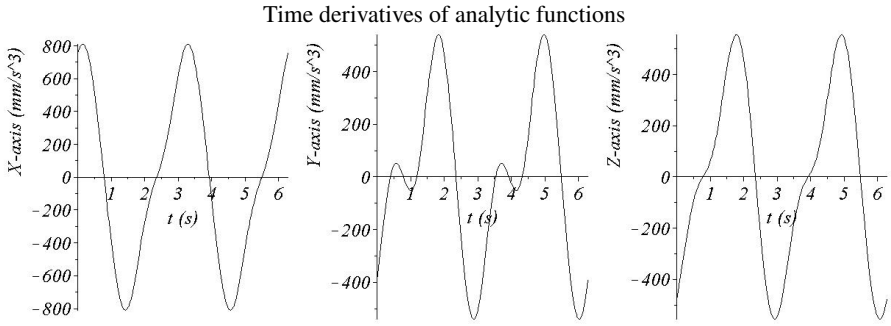

Fig. 15. cont. Time history of the jerk of point O_6 using two different methods. Example 2

physical and geometrical meaning of the obtained expressions is not lost. For example, with the derivation method, the Jacobian matrix is hidden in the obtained expressions and not explicitly as it occurs when the screw theory is applied. This point is of utmost importance when addressing issues such as singularity analysis and the evaluation of the dexterity (manipulability) of robotic manipulators.

6. Conclusions

During the last decades screw theory has established by itself as a reliable tool in the analysis of robotic manipulators and has gained a predominant place in rigid body kinematics. In this paper, the screw theory is applied to the jerk analysis of the PUMA robot, surely one of the most studied manipulators in history and still interesting to investigate. For a better understanding of the contribution, a comprehensive review of concepts involving the Lie algebra $se(3)$ of the Euclidean group $SE(3)$, the Plücker coordinates of lines and of course also the screw algebra which is isomorphic to the motor algebra is provided. The position analysis is included as a preliminary step to the higher-order analyses of the robot. The position analysis is addressed by resorting to the Denavit-Hartenberg convention. The input-output equations of velocity, acceleration and jerk are focused on the end-effector of the PUMA robot, and are valid for both the inverse and the forward analyses of the robot manipulator. Numerical examples illustrate the versatility of the method of kinematic analysis employed in the contribution.

Finally, as far as the authors suppose, the jerk analysis of the PUMA robot by resorting to screw theory has not been approached in previous works. In that sense it is worth mentioning that the acceleration, jerk and in general higher order instantaneous kinematics of robotic manipulators using screw theory have been rather scarce. One of the main advantages of the screw theory is its clear physical and geometrical meaning, which, as proved by the numerical examples, is lost when alternative methods such as the use of time derivatives of analytic functions are used.

References

[1] J. Gallardo-Alvarado. Jerk distribution of a 6–3 Gough-Stewart platform. *Proceedings of the Institution of Mechanical Engineers, Part K: Journal of Multi-body Dynamics*, 217(1):77–84, 2003. doi: 10.1243/146441903763049469.

[2] A. Gasparetto, A. Lanzutti, R. Vidoni, and V. Zanotto. Validation of minimum time-jerk algorithms for trajectory planning of industrial robots. *Journal of Mechanisms and Robotics*, 3(3):031003, 2011. doi:10.1115/1.4004017.

[3] S. Vaidyanathan, V. Christos, V.-T. Pham, K. Madhavan, and B.A. Idowu. Adaptive backstepping control, synchronization and circuit simulation of a 3-d novel jerk chaotic system with two hyperbolic sinusoidal nonlinearities. *Archives of Control Sciences*, (3), 2014. doi: 10.2478/acsc-2014-0022.

[4] M.l Kleer, A. Gizatullin, K. Drebler, and S. Muller. Real-time human in the loop MBS simulation in the fraunhofer robot-based driving simulator. *Archive of Mechanical Engineering*, 61(2):269–285, 2014. doi: 10.2478/meceng-2014-0016.

[5] K. Zboiński and P. Woznica. Optimization of polynomial transition curves from the viewpoint of jerk value. *Archives of Civil Engineering*, (1):181–199, 2017. doi: 10.1515/ace-2017-0012.

[6] Y.-S. Lu and Y.-Y. Lin. Smooth motion control of rigid robotic manipulators with constraints on high-order kinematic variables. *Mechatronics*, 49:11–25, 2018. doi: 10.1016/j.mechatronics.2017.11.003.

[7] J. Huang, P. Hu, K. Wu, and M. Zeng. Optimal time-jerk trajectory planning for industrial robots. *Mechanism and Machine Theory*, 121:530–544, 2018. doi: 10.1016/j.mechmachtheory.2017.11.006.

[8] D. Condurache. Higher-order relative kinematics of rigid body and multibody systems. a novel approach with real and dual Lie algebras. *Mechanism and Machine Theory*, 176:104999, 2022. doi: 10.1016/j.mechmachtheory.2022.104999.

[9] S. Vaidyanathan, K. Benkouider, and A. Sambas. A new multistable jerk chaotic system, its bifurcation analysis, backstepping control-based synchronization design and circuit simulation. *Archives of Control Sciences*, 32(1):123–152, 2022. doi: 10.24425/acs.2022.140868.

[10] V. Loveikin, Y. Romasevych, A. Loveilin, M. Korobko, and A. Liashko. Minimization of oscillations of the tower crane slewing mechanism in the steady-state mode of trolley movement. *Archive of Mechanical Engineering*, 70(3):367–385, 2023. doi: 10.24425/ame.2023.146847.

[11] H.J. Sommer. Kinematic jerk and jounce for multibody dynamics with joint constraints. *Mechanism and Machine Theory*, 196:105613, 2024. doi: 10.1016/j.mechmachtheory.2024.105613.

[12] S.F. Al-Azzawi. Dynamical behavior of a new jerk system inspired from chaotic memory oscillators. *Archives of Control Sciences*, 34(1):149–170, 2024. doi: 10.24425/acs.2024.149656.

[13] D.P. Chevallier. Lie algebras, modules, dual quaternions and algebraic methods in kinematics. *Mechanism and Machine Theory*, 26(6):613–627, 1991. doi: 10.1016/0094-114X(91)90043-4.

[14] R.S. Ball. *The Theory of Screws: A Study in the Dynamics of a Rigid Body*. Hodges, Foster, and Company, 1876.

[15] L. Brand. *Vector and Tensor Analysis*. John Wiley & Sons, New York, 1947.

[16] J.M. Rico, J. Gallardo, and J. Duffy. Screw theory and higher order kinematic analysis of open serial and closed chains. *Mechanism and Machine Theory*, 34(4):559–586, 1999. doi: 10.1016/S0094-114X(98)00029-9.

[17] J. Gallardo-Alvarado. Jerk analysis of a six-degrees-of-freedom three-legged parallel manipulator. *Robotics and Computer-Integrated Manufacturing*, 28(2):220–226, 2012. doi: 10.1016/j.rcim.2011.09.002.

[18] J. Gallardo-Alvarado. *Kinematic Analysis of Parallel Manipulators by Algebraic Screw Theory*. Springer Cham, 2016.

[19] K. Sugimoto and J. Duffy. Application of linear algebra to screw systems. *Mechanism and Machine Theory*, 17(1):73–83, 1982. doi: 10.1016/0094-114X(82)90025-8.

[20] J.M. Rico-Martinez and J. Duffy. An application of screw algebra to the acceleration analysis of serial chains. *Mechanism and Machine Theory*, 31(4):445–457, 1996. doi: 10.1016/0094-114X(95)00089-H.

[21] M.B. Leahy, K.P. Valavanis, and G.N. Saridis. Evaluation of dynamic models for PUMA robot control. *IEEE Transactions on Robotics and Automation*, 5(2):242–245, 1989. doi: 10.1109/70.88046.

[22] D. Condurache. Higher-order kinematics in dual Lie algebra. In F. Bulnes, editor, *Advances on Tensor Analysis and their Applications*, chapter 7, pages 1–25. IntechOpen, Rijeka, 2020.

[23] D. Condurache. Higher-order relative kinematics of rigid body and multibody systems. A novel approach with real and dual Lie algebras. *Mechanism and Machine Theory*, 176:104999, 2022. doi: 10.1016/j.mechmachtheory.2022.104999.

[24] X. Wang, C. Liu, H. Sun, and H. Song. A two-step solution for robot-world calibration made intelligible by implementing Chasles' motion decomposition in Ad(SE(3)). *Mechanism and Machine Theory*, 191:105522, 2024. doi: 10.1016/j.mechmachtheory.2023.105522.

[25] R. Featherstone. Position and velocity transformations between robot end-effector coordinates and joint angles. *The International Journal of Robotics Research*, 2(2):35–45, 1983. doi: 10.1177/027836498300200203.

[26] M.V. Kirdanski and M. Dj. Boric. Symbolic singular value decomposition for a PUMA robot and its application to a robot operation near singularities. *The International Journal of Robotics Research*, 12(5):460–472, 1993. doi: 10.1177/027836499301200506.

[27] N. Mohan, A. Thomas, P.P. Prasanth, M.S. Midhun, and James J, Kurian. Inverse kinematic analysis of PUMA 560 for vision systems. In A.N.R. Reddy, D. Marla, M.N. Favorskaya, and S.Ch.Satapathy, editors, *Intelligent Manufacturing and Energy Sustainability*, pages 285–293, Singapore, 2022. Springer Singapore. doi: 10.1007/978-981-16-6482-3_29.

[28] X. Zhou, Y. Xian, Y. Chen, T. Chen, L. Yang, S. Chen, and J. Huang. An improved inverse kinematics solution for 6-DOF robot manipulators with offset wrists. *Robotica*, 40(7):2275–2294, 2022. doi: 10.1017/S0263574721001648.

[29] F. Xiao, G. Li, D. Jiang, Y. Xie, J. Yun, Y. Liu, L. Huang, and Z. Fang. An effective and unified method to derive the inverse kinematics formulas of general six-DOF manipulator with simple geometry. *Mechanism and Machine Theory*, 159:104265, 2021. doi: 10.1016/j.mechmachtheory.2021.104265.

[30] P. Golla, S. Ramesh, and S. Bandyopadhyay. Kinematics of the hybrid 6-axis (H6A) manipulator. *Robotica*, 41(8):2251–2282, 2023. doi: 10.1017/S0263574723000334.

[31] J.J. Craig. *Introduction to Robotics: Mechanics & Control*. Addison-Wesley Publishing Company, 1985.

[32] S. Elgazzar. Efficient kinematic transformations for the PUMA 560 robot. *IEEE Journal on Robotics and Automation*, 1(3):142–151, 1985. doi: 10.1109/JRA.1985.1087013.

[33] M. Raghavan and B. Roth. Inverse kinematics of the general 6R manipulator and related linkages. *ASME Journal of Mechanical Design*, 115(3):502–508, 1993. doi: 10.1115/1.2919218.

[34] D. Manocha and J.F. Canny. Efficient inverse kinematics for general 6R manipulators. *IEEE Transactions on Robotics and Automation*, 10(5):648–657, 1994. doi: 10.1109/70.326569.

[35] S. Kucuk and Z. Bingul. The inverse kinematics solutions of industrial robot manipulators. In *Proceedings of the IEEE International Conference on Mechatronics, 2004. ICM '04.*, pages 274–279, 2004. doi: 10.1109/ICMECH.2004.1364451.

[36] M.A. Gonzalez-Palacios. The unified orthogonal architecture of industrial serial manipulators. *Robotics and Computer-Integrated Manufacturing*, 29(1):257–271, 2013. doi: 10.1016/j.rcim.2012.06.006.

[37] F. Chen and J. Hehua. Applications of an improved Dixon elimination method for the inverse kinematics of 6R manipulators. *Applied Mathematical Modelling*, 107:764–781, 2022. doi: 10.1016/j.apm.2022.03.006.

[38] J.M. Rico, J. Gallardo A., and J. Duffy. A determination of singular configurations of serial non-redundant manipulators, and their escapement from singularities using Lie products. In J.-P. Merlet and B. Ravani, editors, *Computational Kinematics '95*, pages 143–152, Dordrecht, 1995. Springer Netherlands.

[39] X. Zhang and G. Shi. Multi-objective optimal trajectory planning for manipulators in the presence of obstacles. *Robotica*, 40(4):888–906, 2022. doi: 10.1017/S0263574721000886.

[40] J.J. Craig. *Introduction to Robotics, Global Edition*. Pearson Education, 2021.